






Original Article


Numerical simulation on the stability of rock slope based on an improved SPH Method


YU Shu-yang^{1, 2}  <https://orcid.org/0000-0001-5479-1192>; e-mail: yushuyang_hhu@163.com

REN Xu-hua^{1*}  <https://orcid.org/0000-0003-3903-1333>;  e-mail: renxh@hhu.edu.cn

ZHANG Ji-xun¹  <https://orcid.org/0000-0002-6809-6227>; e-mail: zhangjixun@hhu.edu.cn

WANG Hai-jun³  <https://orcid.org/0000-0003-3134-5602>; e-mail: hjwang@nhri.cn

SUN Zhao-hua²  <https://orcid.org/0000-0002-2410-3309>; e-mail: huahuadeshuijingyu@126.com

ZHOU Yu⁴  <https://orcid.org/0000-0001-8436-8766>; e-mail: yu.zhou.19921105@gmail.com

*Corresponding author

¹ College of Water Conservancy and Hydropower Engineering, Hohai University, Nanjing 210098, China

² School of Transportation and Civil Engineering, Nantong University, Nantong 226019, China

³ State Key Laboratory of Hydrology-Water Resource and Hydraulic Engineering, Nanjing Hydraulic Research Institute, Nanjing 210029, China

⁴ Rock Mechanics and Geo-Hazards Center, Shaoxing University, Shaoxing 312000, China

Citation: Yu SY, Ren XH, Zhang JX, et al. (2021) Numerical simulation on the stability of rock slope based on an improved SPH Method. Journal of Mountain Science 18(7). <https://doi.org/10.1007/s11629-021-6739-x>

© Science Press, Institute of Mountain Hazards and Environment, CAS and Springer-Verlag GmbH Germany, part of Springer Nature 2021

Abstract: The presence of random fissures has a great impact on rock slope stability. To investigate the failure modes and stability of rock slopes containing different types of pre-existing fissures, the fracture mark ξ was introduced to improve the kernel function in the traditional smoothed particle dynamics (SPH) method, and a novel numerical method, the improved kernel of smoothed particle hydrodynamics (IKSPH), was proposed to realise the microscopic damage characteristics of particles. The ‘random fissure generating method’ has been proposed for random fissure generation, and the gravity increase method has been embedded into the IKSPH program, thereby realising the stability analysis of rock slopes considering crack propagation processes. A typical steep rock slope is taken as a numerical simulation example considering the random distributions of pre-existing fissures, and its failure modes as well as the

stability under different conditions were simulated. The results show that the failure processes of the rock slope contain propagations of microcracks and then macrocrack penetrations. When the fissure length is short, shallow collapse failure modes can be observed; when the fissure length is long, the deep layer slide occurs, and the slope stability decreases with an increase in fissure length. The micro and macrocrack surfaces are basically consistent with pre-existing fissure angles, and the safety factor is the least at a fissure angle of 30°. The greater the fissure density, the greater the number of macrocracks, and the stability decreases with an increase in the number of pre-existing fissures. The research results can provide some references for disaster protection and understanding the failure laws of rock slopes. Meanwhile, combining the geological survey results with the numerical simulations and developing a high-performance IKSPH program will be a future research direction.

Received: 16-Feb-2021

Revised: 30-Mar-2021

Accepted: 07-May-2021

Keywords: IKSPH method; Random fissures; Gravity increase method; High rock slopes; Crack propagation; Numerical simulation

1 Introduction

As the weak parts of rock masses, cracks and joints influence the strength and deformation characteristics of rock structures, which are regarded as key factors contributing to rock failure (Liu et al. 2020; Taheri et al. 2020). There are many complex joints and fissures on rock slopes. Under complex boundary conditions, stress concentrates at the crack tips, resulting in the extension of pre-existing fissures, and subsequent overall slope instability (Tao et al. 2020; Yu et al. 2019; Zhang et al. 2020; Zhang et al. 2020; Zhang et al. 2020). Many mining and slope engineering failures are caused by pre-existing fissure propagation and rock bridge connection, such as the Gong Jia Fang landslide in the Three Gorges Reservoir (Tan et al. 2015), and the collapse of the Honglianchi Iron Mine in Hefeng, Hubei Province (Wang et al. 2016). Therefore, understanding the mechanisms and laws of fissured rock masses will be of great significance for rock slope disaster prevention.

Previous progress on the failure modes of fissured rock slopes has mainly concentrated on experimental investigations, theoretical studies, and numerical simulations. Experimental investigations can directly observe the real interaction processes between joints and fissures in rock slopes to infer the physical and mechanical properties of fractured rock masses. For example, Fan et al. (2015) conducted a large-scale shaking table test of rock slopes with muddy joints, and the dynamic characteristics were obtained, and Guo et al. (2016) conducted an experimental study on the seismic dynamic response laws of rock slopes containing anchor bolts. Nevertheless, experimental investigations have the disadvantages of long time periods and high costs; moreover, the test results are discrete, repeatability is difficult, and the existing experimental results are limited to small scales (Wong et al. 2001). Meanwhile, the internal mechanisms of the joint and fissure interactions cannot be directly exhibited. Based on the experimental results, many scholars have tried to express the theory behind overlapping behaviours of multi-fractured rock masses, for example, Horri et al. (1985) deduced the stress intensity factors of parallel

double cracks under axial tension using the Kachanov method, and the interaction laws of crack tips at different horizontal and vertical distances were studied. Zhu et al. (2002) studied the interactions between two random plane cracks by using the Schwarz substitution method, and Chen et al. (2012) derived solutions of multiple cracks in an infinite plate using the Fredholm integral equations. However, theoretical models can only solve some problems with relatively simple boundary conditions, and complex fracture networks will lead to extremely complex mathematical expressions.

As the 'third method of scientific research' (Tang et al. 2006), numerical simulation can not only verify the rationality of experiments and theories, but also clarify the theoretical framework of joint and fissure interactions under different loading conditions. Therefore, many numerical methods have been developed and applied to the analysis of crack propagation and rock slope stability. The finite element method (FEM) is one of the earliest methods for analysing rock slope stability. However, for those problems containing complex pre-existing fissures, FEM needs to re-mesh the crack tip area at every time step, which leads to unexpected calculation terminations (Branco et al. 2015), making the applications inconvenient. As a mesh-less numerical method, the discrete element method (DEM) can realise the interactions between different particles by establishing various contact models to reflect macroscopic fracture laws (Zhang et al. 2012). Therefore, DEM can model the processes of fracture overlap and block slips of rock slopes. However, DEM has many mesoscopic parameters, which have no physical meaning, and it is difficult to calibrate the complex parameters before numerical simulation, which cannot be applied directly to actual engineering (Haeri et al. 2017). Recently, many new numerical methods have been developed to analyse the stability of jointed rock slopes, such as the numerical manifold method (NMM) (Ohnishi et al. 2014; Miki et al. 2010), PeriDynamics (PD) (Shou et al. 2016; Zhou et al. 2016), the phase-field method (Nguyen et al. 2020; Li et al. 2020), and the material point method (MPM) (Müller et al. 2019), all of which have unique advantages in dealing with problems of numerous discontinuities. However, these methods have their own limitations.

In this study, a novel numerical method called the improved kernel of smoothed particle

hydrodynamics (IKSPH) is proposed. By improving the kernel function in the traditional smoothed particle dynamics (SPH) method, the crack propagation processes of rock slopes can be realised, and compared with previous numerical treatments, the stress components of the base particles do not need to be mapped to the stress bond, which reduces the programming load. In view of the lack of analysis on the mechanical characteristics of random fissures (Li et al. 2020), the random fissure generation method (RFGM), which is suitable for IKSPH, is proposed. Meanwhile, the gravity increase method is embedded into the IKSPH program, which can realise the crack propagation processes of rock slopes under gravity loading. One typical steep rock slope in western China is taken as a numerical example, and the crack propagation processes as well as the slope failure modes are simulated. The pre-existing fissure density, dip angles, and lengths are also considered. The research results can provide some references for understanding the failure mechanisms of steep slopes and the prevention of slope disasters.

2 Theory of IKSPH

2.1 Governing equations

Every particle in the IKSPH program should follow four basic equations: (1) continuity, (2) momentum, (3) energy, and (4) motion. They can be written as follows:

$$\left\{ \begin{aligned} \frac{d\rho_i}{dt} &= \sum_{j=1}^N m_j v_{ij}^\beta \frac{\partial W_{ij,\beta}}{\partial x_i^\beta} \\ \frac{dv_i^\alpha}{dt} &= \sum_{j=1}^N m_j \left(\frac{\sigma_i^{\alpha\beta}}{\rho_i^2} + \frac{\sigma_j^{\alpha\beta}}{\rho_j^2} + T_{ij} \right) \frac{\partial W_{ij,\beta}}{\partial x_i^\beta} \\ \frac{de_i}{dt} &= \frac{1}{2} \sum_{j=1}^N m_j \left(\frac{\sigma_i^{\alpha\beta}}{\rho_i^2} + \frac{\sigma_j^{\alpha\beta}}{\rho_j^2} + T_{ij} \right) v_{ij}^\beta \frac{\partial W_{ij,\beta}}{\partial x_i^\beta} \\ \frac{dx_i^\alpha}{dt} &= v_i^\alpha \end{aligned} \right. \quad (1)$$

where ρ , m , v , x , $\sigma^{\alpha\beta}$, e are the density, mass, velocity, position, total stress tensor, energy of the base particle; α , β are the permutation symbol. t is the calculation time step; T is the artificial viscous part, which can reduce non-physical oscillations during calculations; and W is the kernel function of the IKSPH method.

2.2 Elastic solid equation

Every particle in the IKSPH method utilises the elastic solid equation to calculate the stress components. The total stress tensor $\sigma^{\alpha\beta}$ consists of two parts: the hydrostatic pressure p and shear stress τ , which can be written as

$$\sigma^{\alpha\beta} = -p\delta^{\alpha\beta} + \tau^{\alpha\beta} \quad (2)$$

where δ is the Kronecker symbol, and the hydrostatic pressure p can be obtained from the equation of state (Müller et al. 2019):

$$p = \left(1 - \frac{1}{2}\Gamma\eta\right)p_H + \Gamma\rho e \quad (3)$$

where p_H is the Hugoniot curve function and the Γ is the Gruneisen parameter.

The change in the stress rate can be obtained from the strain and strain rates, which can be expressed as follows:

$$\hat{\tau}_{\alpha\beta} = B(\varepsilon^{\alpha\beta} - \frac{1}{3}\delta^{\alpha\beta}\varepsilon^{\gamma\gamma}) + \tau^{\alpha\gamma}R^{\beta\gamma} + \tau^{\gamma\beta}R^{\alpha\gamma} \quad (4)$$

where $\hat{\tau}$ is the stress rate tensor; ε represents the strain tensor; δ is the kronecker delta; τ is the shear stress tensor; α , β and γ are the permutation symbol; B is the shear modulus, and R is the torsion tensor, which can be written as

$$R^{\alpha\beta} = \frac{1}{2} \left(\frac{\partial v^\alpha}{\partial x^\beta} - \frac{\partial v^\beta}{\partial x^\alpha} \right) \quad (5)$$

2.3 Treatments of particle damage

As shown in Eq. (1), for each particle in IKSPH, the transfer of parameter information is done by the derivative of the kernel function $\partial W_{ij,\beta} / \partial x_i^\beta$, for example, the density, velocity, energy, or position. If the derivative of the kernel function can be improved to eliminate the interactions between particles once the particle is damaged, then the fracture characteristics can be reflected. Based on this concept, the fracture mark ξ is introduced here in IKSPH, and the particle damage treatments are shown in Fig. 1. First, the IKSPH program judges whether the particle is damaged; if so, the fracture mark ξ is set to 0; otherwise, $\xi=1$. The improved kernel function considering the particle damage is defined as D , which can be written as

$$\frac{\partial D_{ij,\beta}}{\partial x_i^\beta} = \xi_i \times \frac{\partial W_{ij,\beta}}{\partial x_i^\beta} \quad (6)$$

Therefore, the improved form of IKSPH governing equations can then be expressed as

$$\left\{ \begin{aligned} \frac{d\rho_i}{dt} &= \sum_{j=1}^N m_j v_{ij}^\beta \frac{\partial D_{ij,\beta}}{\partial x_i^\beta} \\ \frac{dv_i^\alpha}{dt} &= \sum_{j \in S} m_j \left(\frac{\sigma_i^{\alpha\beta}}{\rho_i^2} + \frac{\sigma_j^{\alpha\beta}}{\rho_j^2} + T_{ij} \right) \frac{\partial D_{ij,\beta}}{\partial x_i^\beta} \\ &\quad + \sum_{j \in W} m_j \left(\frac{\sigma_i^{\alpha\beta}}{\rho_i^2} + \frac{\sigma_j^{\alpha\beta}}{\rho_j^2} + T_{ij} \right) \frac{\partial D_{ij,\beta}}{\partial x_i^\beta} \\ \frac{de_i}{dt} &= \frac{1}{2} \left(\sum_{j \in S} m_j \left(\frac{\sigma_i^{\alpha\beta}}{\rho_i^2} + \frac{\sigma_j^{\alpha\beta}}{\rho_j^2} + T_{ij} \right) v_{ij}^\beta \frac{\partial D_{ij,\beta}}{\partial x_i^\beta} \right. \\ &\quad \left. + \sum_{j \in W} m_j \left(\frac{\sigma_i^{\alpha\beta}}{\rho_i^2} + \frac{\sigma_j^{\alpha\beta}}{\rho_j^2} + T_{ij} \right) v_{ij}^\beta \frac{\partial D_{ij,\beta}}{\partial x_i^\beta} \right) \\ \frac{dx_i^\alpha}{dt} &= v_i^\alpha \end{aligned} \right. \quad (7)$$

D represents the improved kernel function considering the particle damage, and m represents the particle mass.

2.4 Fracture criteria

The improved form of the Mohr-Coulomb criterion is selected as the fracture criterion, which has been widely used in previous numerical simulations and has achieved good results (Yang et al. 2016), and can be written as

$$\sigma_f = \sigma_t \quad (8)$$

$$\tau_f = c + \sigma_f \tan \varphi \quad (9)$$

where σ_f and τ_f are the maximum tensile stress and

shear stress, respectively; σ_t is particle tensile strength; c is particle cohesion; and φ is the internal friction angle of the particle.

2.5 Random fissure generating method (RFGM)

2.5.1 Geometric generation of random fissures

Numerous fissures and joints exist in rock slopes, whose geometries and locations are difficult to determine; however, their spatial distributions follow a macroscopic statistical law. In other words, their geometric parameters (including fissure dip angles, density, and lengths) can be described by a statistical probability density function. In this section, the Monte Carlo method is introduced in IKSPH, and the linear congruence method is used to generate uniformly distributed random numbers, whose recursive formula is expressed as follows:

$$\left\{ \begin{aligned} x_n &= (ax_{n-1} + c) \pmod{M} \\ r_n &= x_n / M \\ \text{Initial value } &x_0 \end{aligned} \right. \quad (10)$$

where M is the modulus, $\text{mod } M$ represents the remainder of M , a is a multiplier, c is the increment, x_0 is the initial value, and r_n is a random number generated between 0 and 1. Therefore, the formula of a random number which complies with the normal distributions can then be expressed as

$$x'_n = \mu_x + \sigma_x \times \sqrt{-2\ln(r_n)} \times \cos(2 \times \pi \times r_n) \quad (11)$$

where μ_x is the mean value and σ_x is the standard deviation. The 2D random fissure can be characterised by its central point coordinate (fx_0, fy_0) , fissure length fl , and fissure dip angle θ . Therefore, its

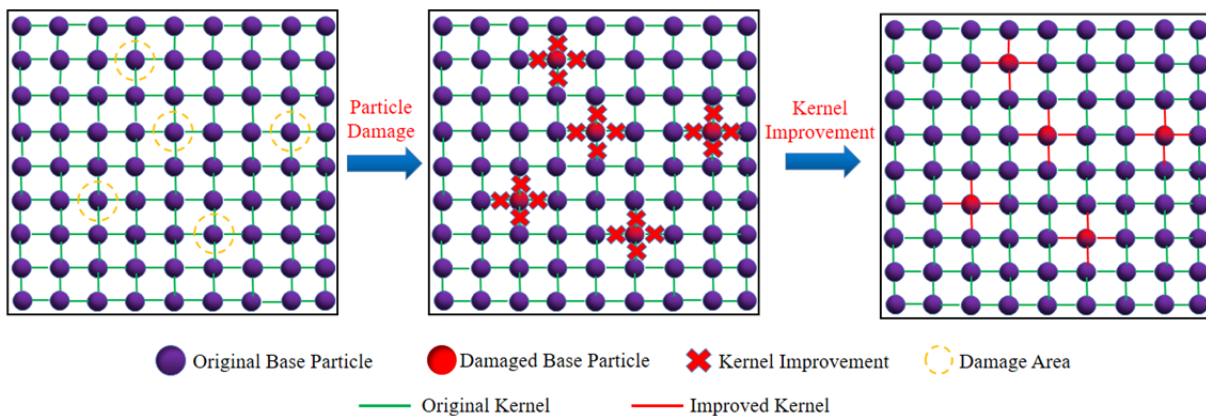


Fig. 1 Damage treatments of particles in improved kernel of smoothed particle hydrodynamics (IKSPH).

endpoints can then be written as

$$\begin{cases} fx = fx_0 \pm (fl/2)\cos\theta \\ fy = fy_0 \pm (fl/2)\sin\theta \end{cases} \quad (12)$$

where fx and fy are the x -direction and y -direction coordinates of random fissure end points, respectively. The fissure density Q can be defined as the ratio of the fissure numbers N to the generation area S . Therefore, the geometric generation processes of random fissures are summarised as follows:

(1) Determine the size of the generation area. It should be noted that when the analysis area shape is irregular, the generation area size is larger than that of the analysis area. Once the generation area is determined, the fissure numbers can then be calculated as $N = Q \times S$.

(2) Determine the random properties of each fissure. N groups of random numbers between 0 and 1 obeying the normal distributions are generated according to Eq. (10), and N groups of fissure central coordinates (fx_0, fy_0) , fissure length fl , and fissure dip angle θ can be generated.

(3) Determine endpoints of each random fissure. According to the fissure parameters generated in step (2), the N groups of random fissure endpoint coordinates (fx, fy) can be calculated using Eq. (11).

2.5.2 Generation strategy of random fissures in IKSPH

Based on the characteristics of IKSPH, a method for generating random fissures is proposed in this section. The schematic diagram is shown in Fig. 2, and the detailed steps are as follows:

(1) First, the endpoints of each fissure are

geometrically located. The endpoint coordinates of the fissures are randomly generated according to the method introduced in Section 2.5.1, which are marked as li ($i=1,2,\dots,n$).

(2) Second, a series of search points are generated on li , which is marked as ni ($i=1,2,\dots,n$). The search radius d is assigned to each search point. It should be stressed that the search radius d should be $1.1 \times$ the average spacing of real particles to ensure searching the target particles.

(3) Finally, for each real particle, if covered by the search radius d , the real particle is marked as a fissure particle, and its derivative of the kernel function is improved according to Eq. (6).

2.6 Gravity increase method embedded in IKSPH

Previous studies on slope stability have mostly utilised the strength reduction method. However, the strength and stability of a rock slope are relatively high, and the gravity increase method has been proven to have the same effect as the strength reduction method (Jiang et al. 2015). Therefore, this section introduces the implementation of the gravity increase method into the IKSPH.

For every IKSPH particle, its external forces include two parts: gravity and the forces of other particles. The gravity action of each particle is realised by gravity acceleration g . Therefore, similar to FEM, the rock slope final instability is caused by increasing the gravity acceleration g of each particle, and the final slope safety factor can be expressed as

$$SF = g_i / g \quad (13)$$

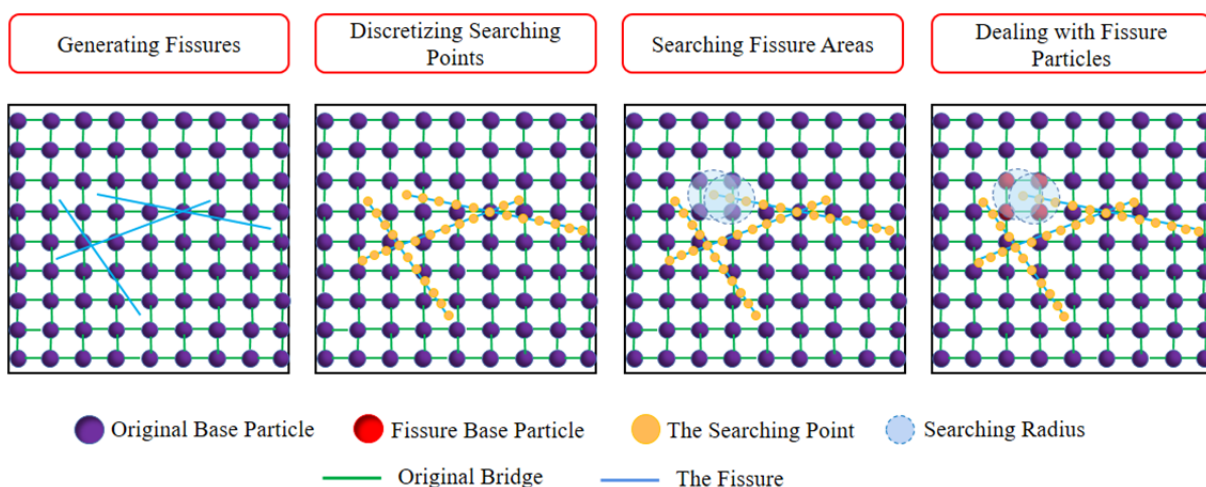


Fig. 2 Generation of random fissures in improved kernel of smoothed particle hydrodynamics (IKSPH).

where SF is the final safety factor of the slope and g_i is the final gravity acceleration.

The criteria for slope instability are as follows: monitor the displacement of the monitoring point at the top of the slope, if the displacement increases rapidly, the slope is considered to be unstable (Fig.3).

3 Numerical Details

3.1 Validation of IKSPH and gravity increase methods

3.1.1 Validation of IKSPH method

To verify the accuracy of the IKSPH method, a numerical model of a cubic specimen with a single crack was established. The model size was $1\text{ m} \times 1\text{ m}$, and one crack with a length of 1 m was prefabricated in the centre with an inclination angle of 45° . A confining pressure of 1 MPa was applied to the model side. The calculation results by IKSPH and Abaqus were consistent, which indicates that the proposed method is accurate and reasonable (Fig.4).

3.1.2 Validation of the gravity increase method

To verify the accuracy of the gravity increase method, a simple slope was calculated by IKSPH and the commercial software Geostudio. The height of the slope was 16 m , the length of the slope was 24 m , and the slope angle was 45° . Fig. 5 shows that the failure shape of the slope calculated by IKSPH is consistent with that of Abaqus. Meanwhile, the safety factor calculated by Geostudio was 2.855 , and the IKSPH result was 2.73 , which verifies the accuracy of the gravity increase method embedded in IKSPH.

3.2 Numerical models

The numerical model is of a rock slope, with a height and length of 486 m and 509 m , respectively. According to the geological survey, the rock strata tend to be along the slope, and the block formed by the cutting of complex joints exhibits a sliding trend. The IKSPH model was established according to a typical slope section. The whole model was divided into 140824 particles, as shown in Fig.6.

3.3 Calculation conditions

Different pre-existing fissure conditions were set

according to the method proposed in Section 2.5: condition A, different fissure lengths l ; condition B, different fissure dip angles θ , and condition C, different fissure density Q , as presented in Table 1. The crack propagation processes and safety factors of the rock slope were calculated.

3.4 Parameter determination

To reflect the inhomogeneity of rock materials, a

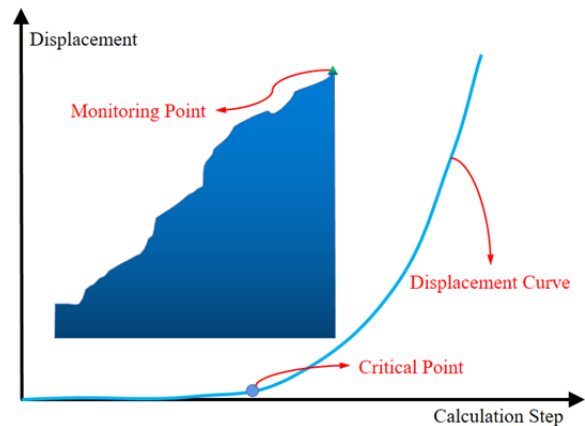


Fig. 3 Discrimination of slope instability by Gravity Increase Method embedded in IKSPH method.

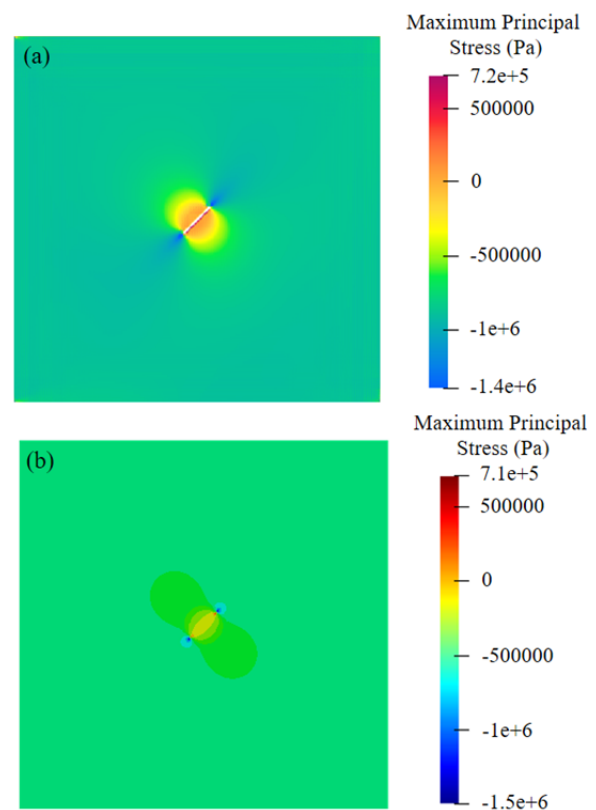


Fig. 4 The maximum principal stress distributions of (a) IKSPH results (b) Abaqus results.

Table 1 Calculation conditions

| Schematic diagram | Number | Details |
|-------------------|--------|-------------------------------------|
| | A1 | $fl=10$ m |
| | A2 | $fl=20$ m |
| | A3 | $fl=30$ m |
| | A4 | $fl=40$ m |
| | B1 | $\theta=15^\circ$ |
| | B2 | $\theta=30^\circ$ |
| | B3 | $\theta=45^\circ$ |
| | B4 | $\theta=60^\circ$ |
| | C1 | $Q=10/(509 \times 486 \text{ m}^2)$ |
| | C2 | $Q=20/(509 \times 486 \text{ m}^2)$ |
| | C3 | $Q=30/(509 \times 486 \text{ m}^2)$ |
| | C4 | $Q=40/(509 \times 486 \text{ m}^2)$ |

heterogeneous coefficient m is introduced here, and the double parameter Wei-bull function is generally used to express the random distribution characteristics of basic parameters (Weibull et al. 1939):

$$f(x) = \frac{m}{x_0} \left(\frac{x}{x_0}\right)^{m-1} \exp\left[-\left(\frac{x}{x_0}\right)^m\right] \quad (14)$$

where x is the basic mechanical parameters of the particles (e.g., modulus of elasticity, compressive strength, cohesion, etc.), x_0 is the mean value of basic mechanical parameters, and m is the heterogeneity extent of particles.

The 2D standard rectangular numerical model was established, the size of which was 50 mm × 100 mm, and the heterogeneous coefficient m was set to 10. The elastic modulus, Poisson's ratio, tensile strength, cohesive strength, and internal friction angle were 0.1 GPa, 0.2, 8 MPa; 2.5 MPa, and 35°, respectively. Through continuous trial calculations, the stress-strain curves and failure modes were developed and are shown in Fig. 7, which are consistent with previous experimental results (Han et al. 2020). Meanwhile, Fig. 8 shows the entire failure processes of the numerical specimen, and the crack initiation and propagation processes can be clearly observed, which indicates that IKSPH has unique advantages in dealing with discontinuous problems.

4 Simulation Results

4.1 Rock slope failure modes

The crack propagation processes are shown in

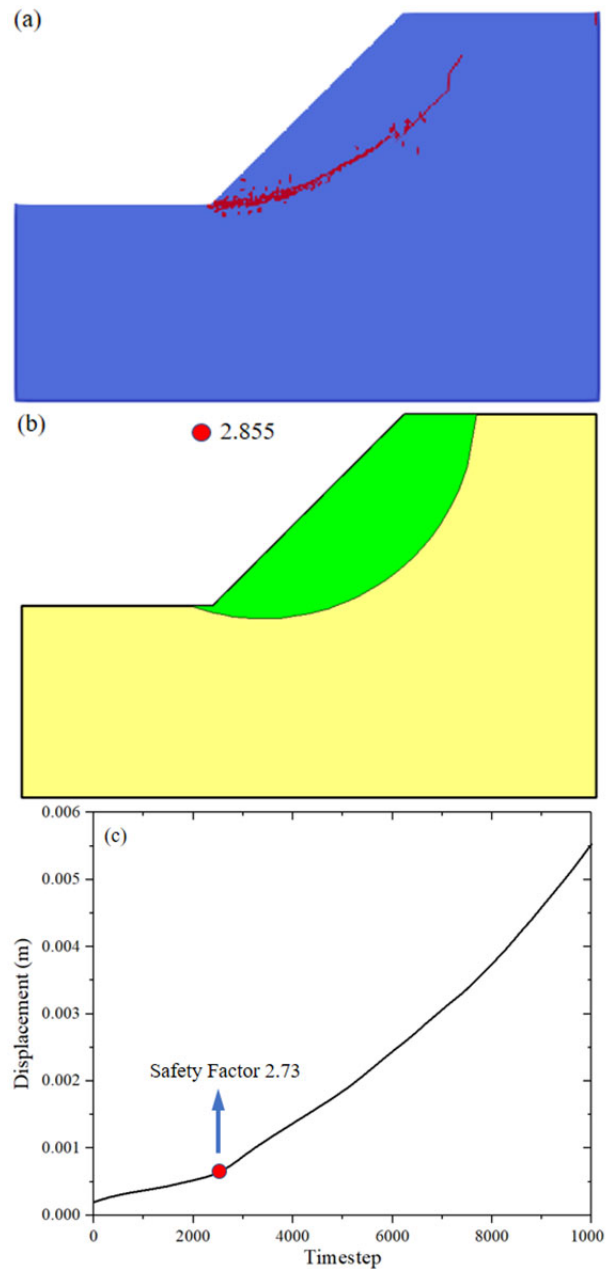


Fig. 5 Verifications of Gravity Increase Method. (a) IKSPH results; (b) Geostudio results; (c) Safety factor of IKSPH.

Appendixes 1–3. It should be stressed that the crack failure modes were distinguished in our simulation. Tensile failure is marked white, while shear failure is marked in red.

4.1.1 Influence of different fissure lengths on slope failure

The rock slope failure was caused by crack propagation of pre-existing fissures (Appendix 1). For short fissure lengths, the cracks propagated along the gravity direction, and typical ‘wing cracks’ were

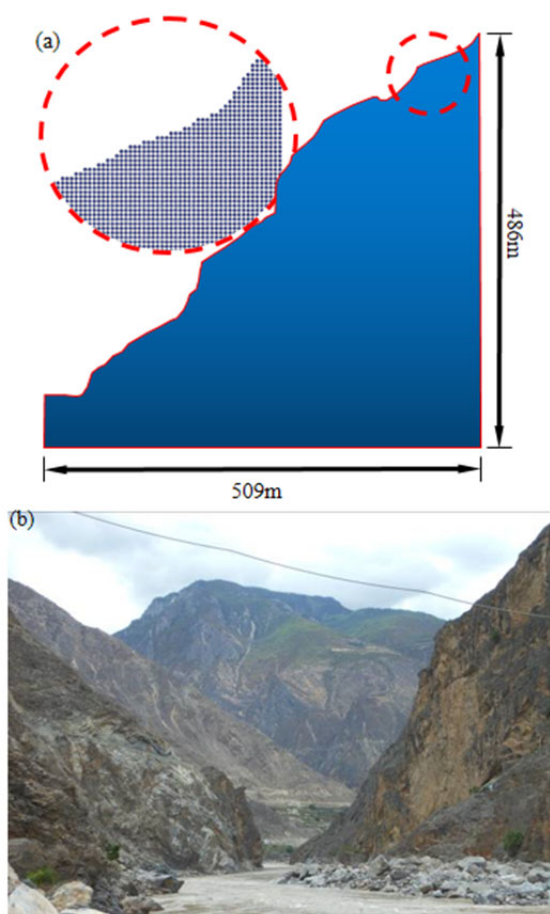


Fig. 6 (a) Numerical model of the rock slope; (b) The actual section of the rock slope.

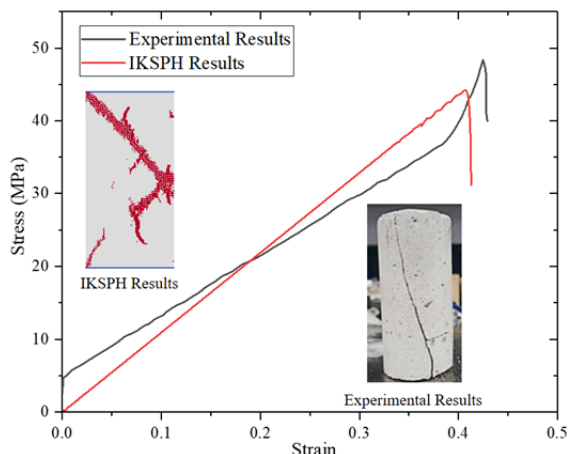


Fig. 7 Comparison between numerical simulation and experimental results.

formed, which could often be observed in previous small-scale specimens (Li et al. 2020). For long fissure lengths, cracks initiated and propagated horizontally and eventually, cracks overlapped, and slope instability occurred. It should be noted that the

first three images of each group are the microcrack propagation processes, and the last image is the macroscopic damage caused by the microcrack propagation. The macroscopic failure surface did not always follow the propagation paths of the microcracks; however, the overall failure trend was consistent with the microcrack directions. Meanwhile, the slope failure mode was mainly shallow (local) collapse when the fissure lengths were short (Appendix 1a). When the fissure lengths were long, the final failure mode was mainly deep failure (Appendix 1b, c, and d). Finally, shear failure mainly occurred on the crack surface, and tensile failure mainly occurred during crack propagation.

4.1.2 Influence of different fissure dip angles on slope failure

From Appendix 2, we inferred that the fissure dip angles determined the directions of micro and macrocracks. For small fissure dip angles (Appendix 2 a, b), the crack initiation followed the directions of pre-existing fissures, and the angle between the macro fracture surface and horizontal direction was not large. With larger fissure dip angles, the microcrack initiation and propagation directions differed from the original fissure dip angles, and the angles between the macrocracks and the horizontal direction were also large.

4.1.3 Influence of different fissure densities on slope failure

The simulation results showed that the fissure densities had a significant impact on the rock slope failure modes (Appendix 3). For the conditions with small fissure densities (Appendix 3a), the microcrack propagation degree was less than that of other conditions. Microcracks initiated not only on the pre-existing fissure tips but also at the slope corners. The final slope failure mode was mainly shallow collapse. For high fissure densities, the interactions between different fissures were stronger, leading to denser fracture networks. The final failure mode was mainly deep failure (Appendix 3b, c, and d).

4.2 Statistics of crack number

The crack number increased slowly during the early simulation stages (Figs. 9–11). However, when the gravity increased to a certain extent, the crack number increased sharply, leading to the final failure of the rock slope. The tensile crack number was

always larger than the shear crack number, which means that the main failure mode of the rock slope is tensile failure.

The total crack numbers of A1–A4 were 4607, 4977, 6193, and 6274, respectively showing an increasing trend, which means that with the increase in the crack length, the rock slope is more unstable. The total number of cracks in B1–B4 was 4952, 2695,

4977, and 5229, which first decreased and then increased, and shows that the most unstable condition is when the fissure angle is equal to 30°. The total number of cracks in C1–C4 was 4607, 4977, 6274, and 6503, also showing an increasing trend, indicating that a large fissure density will be a negative factor for the rock slope stability.

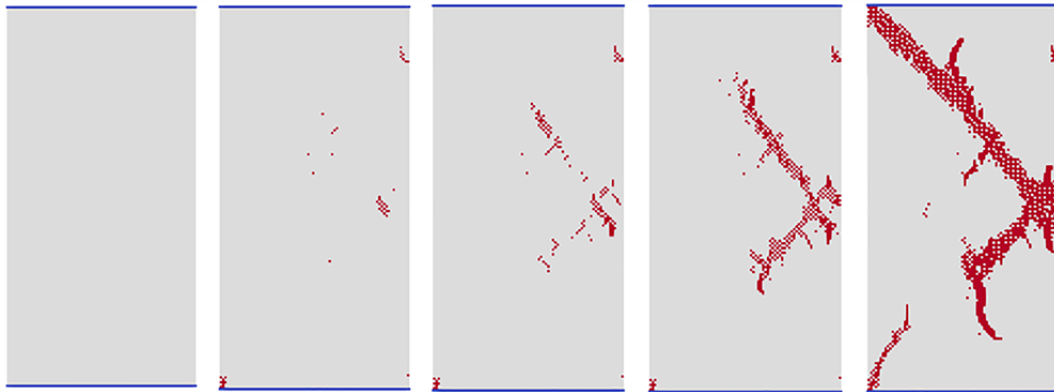


Fig. 8 The failure processes of IKSPH numerical specimen.

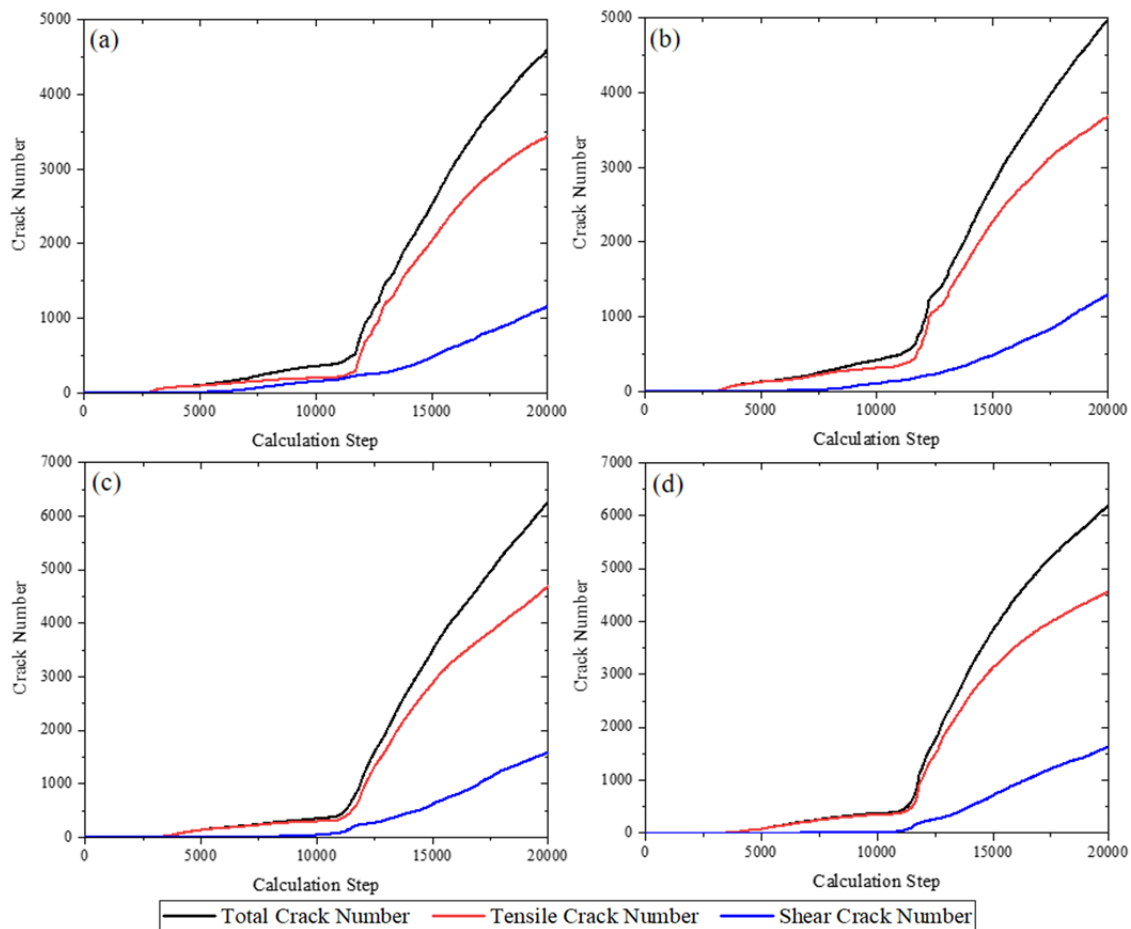


Fig. 9 Crack numbers under condition A. (a) Condition A1; (b) Condition A2; (c) Condition A3; (d) Condition A4.

4.3 Rock slope stability analysis

The slope safety factor varied notably with different fissure properties (Fig. 12). For condition A, the safety factor decreased with an increase in the fissure length, which indicates that an increase in the fissure length will have a negative effect on the stability of the rock slope. For condition B, the safety factor decreased first and then increased with the increase in the dip angles, and reached a minimum in condition B2 (fissure dip angle is 30°), indicating that a dip angle of 30° is the least safe. In condition C, the safety factor decreased with an increase in fissure densities, and there was a dramatic decrease from condition C3 to C4, which indicates that the fissure density $Q=30/(509 \times 486 \text{ m}^2)$ is a critical value of slope stability and instability.

5 Discussions

5.1 Comparisons between the IKSPH results and previous studies

Due to the difficulties in performing large-scale rock slope experiments and the lack of field surveys of pre-existing rock slope fissures, most studies have focused on small-scale specimens. It should be stressed that randomness also exists in our numerical results. However, our simulations can also reflect some basic laws of fissure overlaps, interactions, and propagation, which are also similar to the small-scale experimental results and can validate the IKSPH method.

Fig. 13a, b shows typical ‘wing cracks’ in our simulation results. ‘Wing cracks’ initiate at pre-existing fissure tips under uniaxial compression, and propagate along the direction of maximum principal stress, which has been observed in previous experimental results (Liu et al. 2020). The VIC-3D results showed that fissure surface slip leads to the tensile stress concentration at the fissure tips, forming ‘wing cracks’, as shown in Fig.13c (Liu et al.

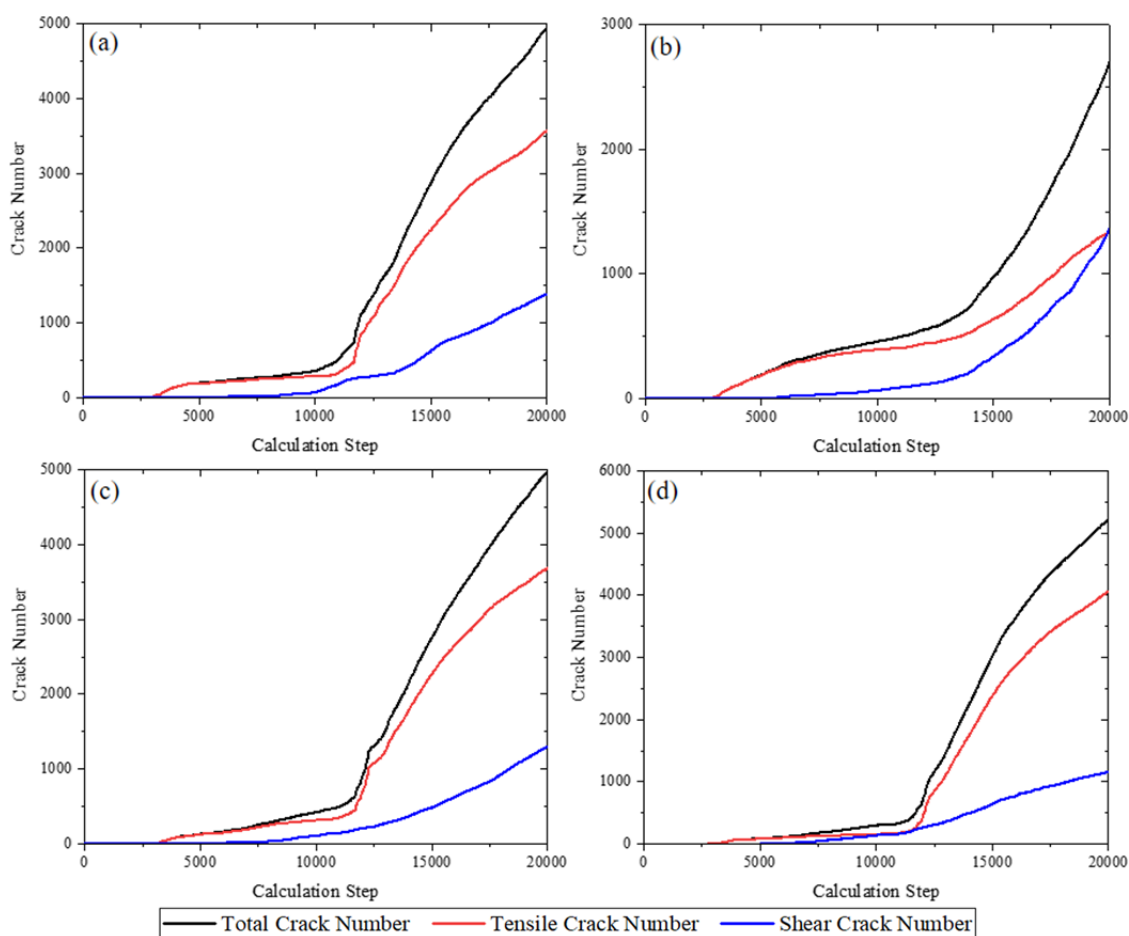


Fig. 10 Crack numbers under condition B. (a) Condition B1; (b) Condition B2; (c) Condition B3; (d) Condition B4.

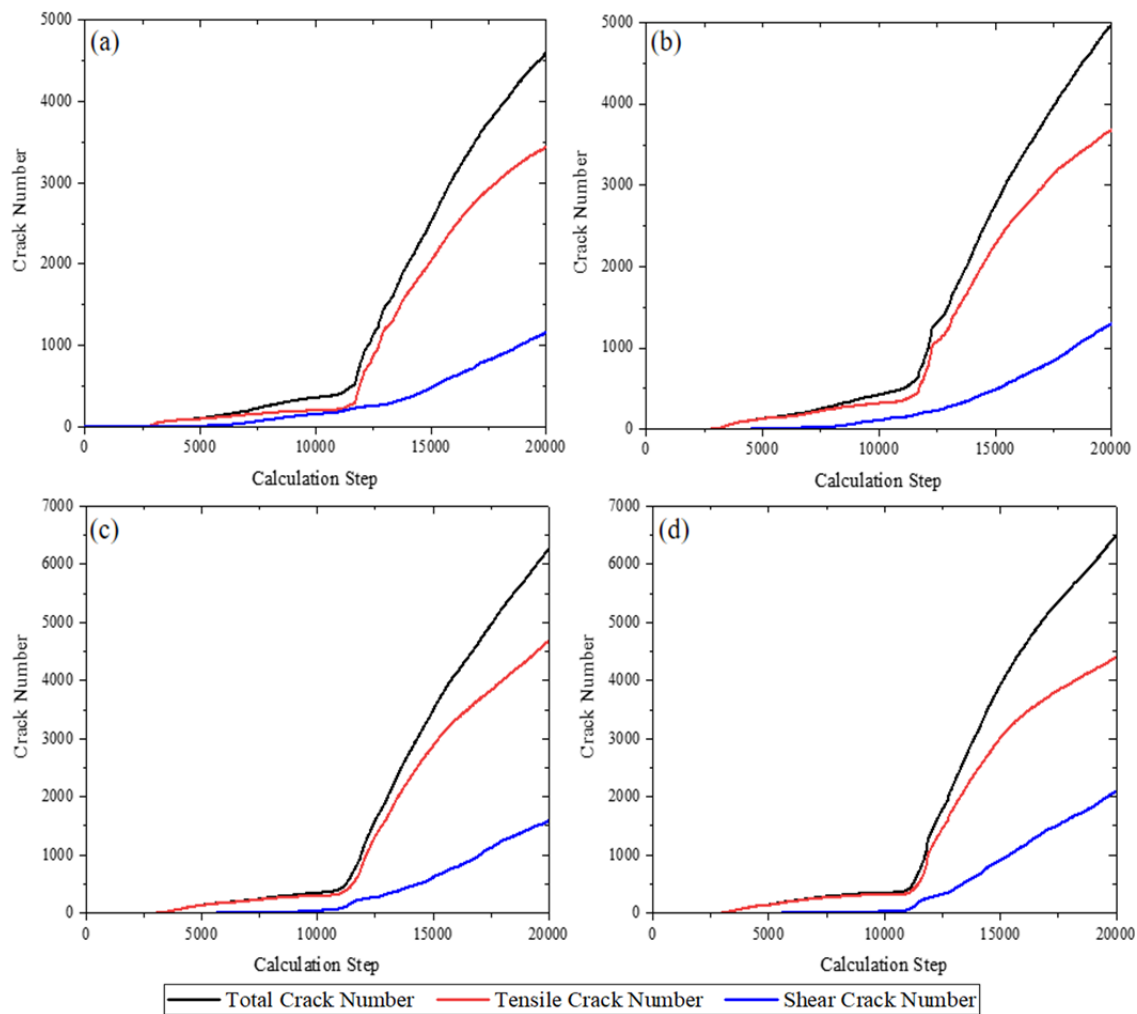


Fig. 11 Crack numbers under condition C. (a) Condition C1; (b) Condition C2; (c) Condition C3; (d) Condition C4.

2020).

The interaction modes of the double fissures differ depending on their positions. Fig. 14a shows the conditions of large overlap degrees. Not only do the ‘wing crack’ initiate from the fissure tips, but also the rock bridges between two fissures are connected, which is similar to the experimental results 1 (Zhu et al. 2017). Fig. 14b shows the interaction characteristics for small overlap degrees. ‘Wing cracks’ initiate from the outer sides of the fissures, and the ‘wing cracks’ of the inner sides connect, which is also consistent with experimental results 2 (Zhu et al. 2017).

5.2 Application prospects of IKSPH method in stability evaluation of rock slopes

In our work, by improving the kernel function in the traditional SPH method, mesoscopic particle

damage is achieved. Meanwhile, the RFGM has been put forward to realise the generations of random distributed fissures in rock slopes. The traditional gravity increase method was embedded into the IKSPH program, and the evaluation of rock slope considering crack propagation processes has been realised. Compared with traditional FEM, the proposed method does not depend on the grids and does not need to re-mesh grids during calculation, which can reflect the real conditions of the rock slope failure process. Furthermore, the simulation results are similar to the previous small-scale experimental results. Therefore, the application of the IKSPH method in the evaluation of rock slopes is promising.

However, it should be stressed that previous studies mostly utilised small-scale specimens, and the numerical results are limited due to numerous assumptions (for example, regular distributions of cracks, regular shapes of slopes, etc.), which cannot

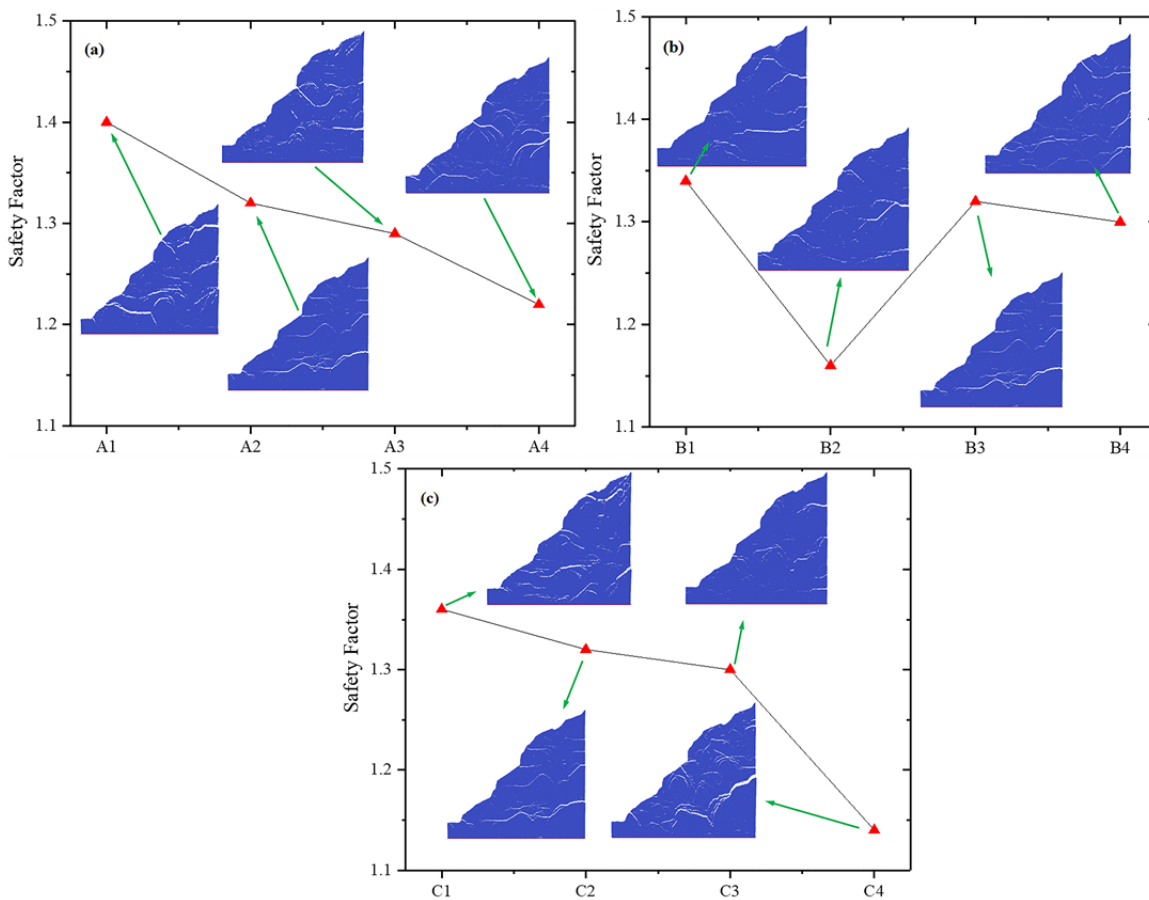


Fig. 12 The stability of the rock slope under different conditions. (a) Condition A: different fissure lengths; (b) Condition B: different fissure dip angles; (c) Condition C: different fissure density.

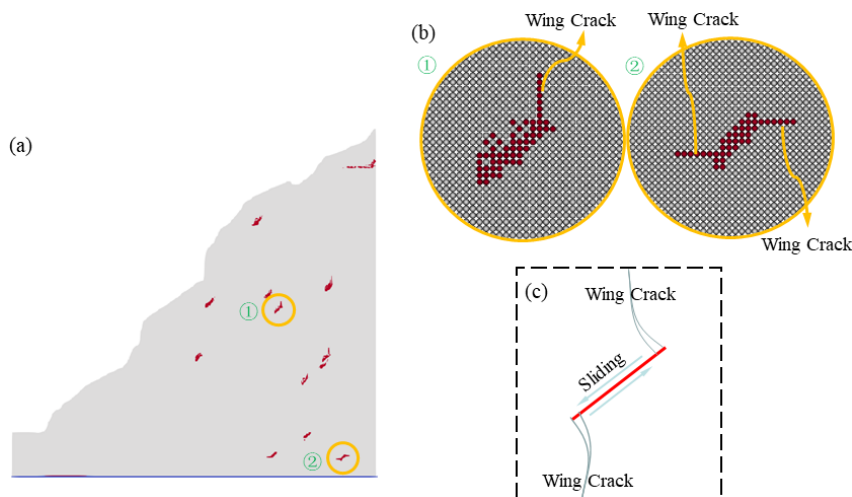


Fig. 13 Comparisons of ‘wing cracks’ between IKSPH results and previous experimental results. (a) IKSPH results of condition A1; (b) ‘Wing crack’ in condition A1; (c) Experimental results of ‘wing crack’ (Liu et al. 2020).

reflect the real states of rock slopes. Our work is a numerical trial of random fissures in a real rock slope. The numerical results cannot completely represent the real conditions, for the following reasons: 1) The physical and mechanical properties of rock slopes

vary widely, which cannot be fully considered in the numerical simulation; 2) The failure modes and stability of rock slopes are greatly affected by fissure locations and properties, and the distributions of pre-existing fissures in our simulation cannot be

consistent with real conditions. Therefore, combining the geological survey results with numerical simulations will be the focus of future research. Meanwhile, practical engineering problems are mostly 3D problems, and the simplified 2D model cannot fully represent 3D problems. In addition, the computational efficiency of the 3D numerical model was relatively low. Therefore, developing a high-performance 3D IKSPH program will be a future research direction.

6 Conclusions

In this study, we improved the kernel function in the traditional SPH method and proposed a new numerical method called IKSPH, which can simulate rock fracture processes. Meanwhile, we proposed an RFGM and embedded the gravity increase method into the simulation framework. Then, we performed numerical simulations of a rock slope containing random fissures, and the failure modes and discussed the stability under different conditions. The following conclusions were drawn from this work.

(1) Crack propagation in the simulated rock slope contains two stages: the formation of microcracks, where microcracks initiate and propagate, and the formation of macro fractures, where macrocracks occur and the rock slope fails. The macroscopic failure surface does not always follow the propagation paths of the microcracks; however, the overall failure trend is consistent with the microcrack directions.

(2) The rock slope failure modes were significantly influenced by the fissure properties. Short fissure lengths lead to shallow collapse failure modes, whereas long fissure lengths lead to deep layer slide failure modes. The fissure angle dominates the strike of the macrocrack, and the propagation angles of the macrocracks increase with the increase in pre-existing random fissures. When the fissure density was small, the microcrack fragmentations were small;

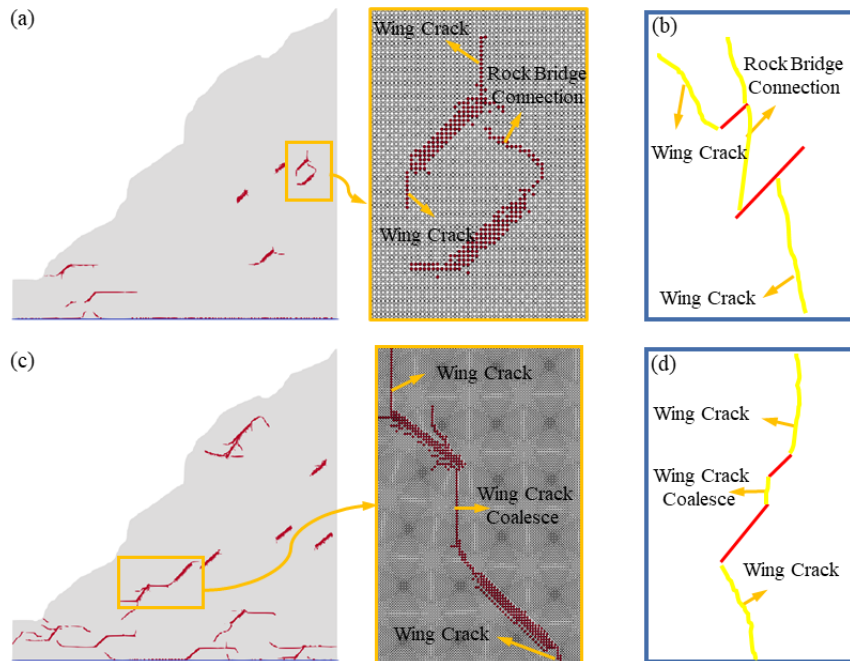


Fig. 14 Comparisons of double fissure connections between IKSPH results and previous experimental results. (a) IKSPH results of condition C1; (b) Experimental results 1 (Zhu et al. 2017); (c) IKSPH results of condition A3; (d) Experimental results 2 (Zhu et al. 2017).

however, when the fissure density was large, the microcrack fragmentation increased sharply.

(3) The fissure properties also significantly impacted the rock slope stability. The increase in fissure lengths and densities decreased the rock slope stability. Meanwhile, SF first decreased and then increased with an increase in fissure angles.

Notably, the present study only performed highly simplified examples to illustrate that IKSPH can be applied to rock slope stability analysis. Actual engineering practices are complex 3D problems. Therefore, the geological survey results with numerical simulations and the development of a 3D high-performance IKSPH program will be a future research direction.

Acknowledgements

The research reported in this manuscript is funded by the the National Natural Science Fund (Grant No. U1765204, 51409170) and the Fundamental Research Funds for the Central Universities of China (B210203078).

Electronic supplementary material: Supplementary material (Appendixes 1-3) is available in the online version of this article at <https://doi.org/10.1007/s11629-021-6739-x>.

References

- Branco R, Antunes F, Costa J (2015) A review on 3D-FE adaptive remeshing techniques for crack growth modelling. *Eng Fract Mech* 141: 170-195. <https://doi.org/10.1016/j.engfracmech.2015.05.023>
- Chen W (2012) Theory and application of stability analysis for underground engineering of fractured rock mass. Science Press. pp 75-82. (In Chinese)
- Fan G, Zhang J, Fu X (2015) Study on the difference of dynamic response of bedding and anti-dumping rock slope with muddy intercalation. *Chin J Geotech* 37(04): 692-699. (In Chinese) <https://doi.org/10.11779/CJGE201504015>
- Guo Y, Cao Z, Sheng L (2016) Study on Centrifugal Model for Stress Monitoring of Rock Slope. *J Shandong Univ* 46(02): 101-107. (In Chinese) <https://doi.org/10.6040/j.issn.1672-3961.0.2015.048>
- Horii H, Nemat-Nasser S (1985) Elastic fields of interacting inhomogeneities. *Int J Solids Struct* 21(7): 731-745. [https://doi.org/10.1016/0020-7683\(85\)90076-9](https://doi.org/10.1016/0020-7683(85)90076-9)
- Han W, Jiang Y, Luan H (2020) Numerical investigation on the shear behavior of rock-like materials containing fissure-holes with FEM-CZM method. *Comput Geotech* 125: 103670. <https://doi.org/10.1016/j.compgeo.2020.103670>
- Haeri H, Sarfarazi V, Zhu Z (2017) Effect of normal load on the crack propagation from pre-existing joints using Particle Flow Code (PFC). *Comput Concrete* 19(1): 99-110. <https://doi.org/10.12989/cac.2017.19.1.099>
- Jiang M, Jiang T, Crosta G (2015) Modeling failure of jointed rock slope with two main joint sets using a novel DEM bond contact model. *Eng Geol* 193: 79-96. <https://doi.org/10.1016/j.enggeo.2015.04.013>
- Liu S, Zhang D, Liu H (2020) Rock Crack Propagation Mechanism of Oriented Perforation Hydraulic Fracture under Different Perforation Parameters. *Arab J Sci Eng* 45(10): 8711-8725. <https://doi.org/10.1007/s13369-020-04821-y>
- Li Z, Shou Y, Zhang X (2020) Stability analysis of flawed rock slope by using virtual-bond-based general particles dynamics. *Theor Appl Fract Mech* 108: 102631. <https://doi.org/10.1016/j.tafmec.2020.102631>
- Li W, Nhon N, Zhou K (2020) Phase-field modeling of brittle fracture in a 3D polycrystalline material via an adaptive isogeometric-meshfree approach. *Int J Numer Methods Eng* 121(22): 5042-5065. <https://doi.org/10.1002/nme.6509>
- Li X, Li H, Liu L (2020) Investigating the crack initiation and propagation mechanism in brittle rocks using grain-based finite-discrete element method. *Int J Rock Mech Min Sci* 127: 1-20. <https://doi.org/10.1016/j.ijrmms.2020.104219>
- Liu L, Li H, Li X (2020) Full-field strain evolution and characteristic stress levels of rocks containing a single pre-existing flaw under uniaxial compression. *Bull Eng Geol Environ* 79: 3145-3161. <https://doi.org/10.1007/s10064-020-01764-4>
- Miki S, Sasaki T, Koyama T (2010) Development of coupled Discontinuous Deformation Analysis And Numerical Manifold Method (NMM-DDA). *Int J Comput Methods* 7(01): 131-150. <https://doi.org/10.1142/S021987621000209X>
- Muller, Andre, Vargas E (2019) Stability analysis of a slope under impact of a rock block using the generalized interpolation material point method (GIMP). *Landslides* 16: 751-764. <https://doi.org/10.1007/s10346-018-01131-1>
- Nguyen-Thanh N, Li W, Huang J (2020) Adaptive higher-order phase-field modeling of anisotropic brittle fracture in 3D polycrystalline materials. *Comput Meth Appl Mech Eng* 372(1): 113434. <https://doi.org/10.1016/j.cma.2020.113434>
- Ohnishi Y, Sasaki T, Koyama T (2014). Recent insights into analytical precision and modelling of DDA and NMM for practical problems. *Geomech Eng* 9(2): 97-112. <https://doi.org/10.1080/17486025.2013.871066>
- Shou Y, Zhou X, Qian Q (2016) Dynamic Model of the Zonal Disintegration of Rock Surrounding a Deep Spherical Cavity. *Int J Geomech* 17(6): 04016127. [https://doi.org/10.1061/\(ASCE\)GM.1943-5622.0000824](https://doi.org/10.1061/(ASCE)GM.1943-5622.0000824)
- Taheri A, Zhang Y, Munoz H (2020) Performance of rock crack stress thresholds determination criteria and investigating strength and confining pressure effects. *Constr Build Mater* 20(243): 118263. <https://doi.org/10.1016/j.conbuildmat.2020.118263>
- Tao Z, Liu K, Cui X (2020) Infrared Temperature Law and Deformation Monitoring of Layered Bedding Rock Slope under Static Load. *Adv Civ Eng* 2020(4): 1-16. <https://doi.org/10.1155/2020/8818278>
- Tan J (2015) Study on the Mechanism of Instability and Prevention of Anti-Dumping Layer Embedded Rock-socketed Slope in Three Gorges Reservoir Area. PhD thesis, Chang'an University, Xi'an, Shanxi. p 25 (In Chinese)
- Tang C, Li L, Li C (2006) Analysis of Geotechnical Engineering Stability RFPA Strength Reduction. *Chin J Rock Mech Eng* 2006(08): 1522-1530. (In Chinese) [https://doi.org/10.1016/S1872-1508\(06\)60035-1](https://doi.org/10.1016/S1872-1508(06)60035-1)
- Wang Z, Yan E, Liu J (2016) Analysis on the characteristics of collapse failure and formation mechanism of back-dip rock slope in Honglianchi Iron Mine, Hefeng, Hubei Province. *Chin J Geol Disaster Prev Control* 27(3): 7-13. (In Chinese) <https://doi.org/10.16031/j.cnki.issn.1003-8035.2016.03.02>
- Wong R, Chau K, Tang C (2001) Analysis of crack coalescence in rocklike materials containing three flaws-Part I: experimental approach. *Int J Rock Mech Min Sci* 38: 909-924. [https://doi.org/10.1016/S1365-1609\(01\)00065-X](https://doi.org/10.1016/S1365-1609(01)00065-X)
- Yu S, Ren X, Zhang J (2021) An improved form of smoothed particle hydrodynamics method for crack propagation simulation applied in rock mechanics. *Int J Min Sci Technol* 31: 421-428. <https://doi.org/10.1016/j.ijmst.2021.01.009>
- Yang Y, Tang X, Zheng H, Liu Q, He L (2016) Three-dimensional fracture propagation with numerical manifold method. *Eng Anal Bound Elem* 72: 65-77. <https://doi.org/10.1016/j.enganabound.2016.08.008>
- Yu S, Zhang J, Ren X (2019) Numerical analysis of the seepage characteristics of slopes with weak interlayers under different rainfall levels. *Appl Ecol Environ Res* 17(5): 12465-12478. https://doi.org/10.15666/aer/1705_1246512478
- Zhu W, Li Z, Chen W (2002) Failure mechanism and anchoring effect of jointed rock mass and its engineering application. Science Press. pp 126-182. (In Chinese)
- Huang Y, Yang S, Tian W (2019) Cracking process of a granite specimen that contains multiple pre-existing holes under uniaxial compression. *Fatigue Fract Eng Mater Struct* 42(6): 1341-1356. <https://doi.org/10.1111/ffe.12990>
- Zhou X, Shou Y (2016) Numerical simulation of failure of rock-like material subjected to compressive loads using improved Peridynamic method. *Int J Geomech* 2016: 04016086. [https://doi.org/10.1061/\(ASCE\)GM.1943-5622.0000778](https://doi.org/10.1061/(ASCE)GM.1943-5622.0000778)
- Zhu D, Chen Z, Xi J (2017) Analysis on interaction law of parallel offset cracks in rock. *Chin J Geotech Eng* 39(02): 235-243. (In Chinese) <https://doi.org/10.11779/CJGE201702006>
- Zhang Y, Zhang Z, Xue S (2020) Stability analysis of a typical landslide mass in the Three Gorges Reservoir under varying reservoir water levels. *Environ Earth Sci* 79(1): 42. <https://doi.org/10.1007/s12665-019-8779-x>
- Zhang Y, Tang J, He Z (2020) A novel displacement prediction method using gated recurrent unit model with time series analysis in the Erdaohe landslide. *Nat Hazards* 105: 783-813. <https://doi.org/10.1007/s11069-020-04337-6>
- Zhang Y, Tang J, Zhang M (2020) Application of an enhanced BP neural network model with water cycle algorithm on landslide prediction. *Stoch Environ Res Risk Assess* 12: 185-198. <https://doi.org/10.1007/s00477-020-01920-y>